



HAL
open science

Fast Padé transform in the theory of resonances: exact solution of the harmonic inversion problem

Dževad Belkić, Karen Belkić

► **To cite this version:**

Dževad Belkić, Karen Belkić. Fast Padé transform in the theory of resonances: exact solution of the harmonic inversion problem. *Journal of Physics B: Atomic, Molecular and Optical Physics*, 2011, 44 (12), pp.125002. 10.1088/0953-4075/44/12/125002 . hal-00627151

HAL Id: hal-00627151

<https://hal.science/hal-00627151>

Submitted on 28 Sep 2011

HAL is a multi-disciplinary open access archive for the deposit and dissemination of scientific research documents, whether they are published or not. The documents may come from teaching and research institutions in France or abroad, or from public or private research centers.

L'archive ouverte pluridisciplinaire **HAL**, est destinée au dépôt et à la diffusion de documents scientifiques de niveau recherche, publiés ou non, émanant des établissements d'enseignement et de recherche français ou étrangers, des laboratoires publics ou privés.

Fast Padé Transform in the Theory of Resonances: Exact Solution of the Harmonic Inversion Problem

Dževad Belkić and Karen Belkić

Karolinska Institute, P.O. Box 260, S-171 76 Stockholm, Sweden

Abstract: We present the fast Padé transform (FPT) as a polynomial quotient for the Green or response function from signal processing, spectroscopy and resonant scattering theory. Specific illustrations are given for nuclear magnetic resonance spectroscopy within the problem of harmonic inversion, quantification or spectral analysis. Here, the input time signal points or auto-correlation functions are given via measurements or computations, and the task is to reconstruct the unknown components as the harmonic variables in terms of the fundamental complex frequencies and amplitudes. The FPT solves the harmonic inverse problem exactly by retrieving the true number of resonances with all their proper spectral parameters. This output list is finalized by means of Froissart doublets or poles-zero confluences for unequivocal disentangling of the physical/genuine from unphysical/spurious contents of the analyzed time signal. Stability of investigated systems under external perturbations is especially challenged by the presence of noise. The FPT can assess the system's stability through determining the locations and distributions of spectral poles and zeros in the complex frequency plane. This permits identification of the regions that are void of noise. Hence the possibility for improved system's performance under more stable conditions with full signal-noise separation. The FPT can provide a number of important biophysical and chemical quantities, including the density of states and abundance or concentrations of all the physical constituents from the investigated substance.

1 Introduction

We study the quantification problem for general time signals and their spectra. The illustrations are given for data from nuclear magnetic resonance spectroscopy (MRS) [1]–[6]. The quantification (or harmonic inversion) problem entails using the input time signals to reconstruct the true number of resonances as well as all the constituent physical transients (harmonics) together with the pairs of spectral parameters that are complex-valued frequencies and the corresponding amplitudes [2]. Moreover, every time signal has a structure which is quantifiable by a relatively limited number of parameters. In practice, neither this structure nor the related parameters of the studied time signals are known prior to signal processing. The task of spectral synthesis is to reconstruct these unknown quantities from the given time signal, and this is achieved by performing spectral decomposition. To this end a number of methods can be used [7]–[14]. We presently achieve this goal by using the non-linear parametric signal processor called the fast Padé transform (FPT) [15]–[17]. For the given Maclaurin series, a frequency spectrum in the FPT is defined by the unique ratio of two polynomials P_K/Q_K , where K is the total number of resonances (genuine plus spurious). The fast Fourier transform (FFT), with its spectrum given by a single Riemann polynomial R_N , where N is the total signal length, cannot solve this quantification problem. This occurs because the FFT ignores the structure of the investigated time signal. There are two kinds of spectral shapes in signal processing. These are the component shape spectra for each separate resonance and the total shape spectrum as the sum of all the separate component shape spectra, resulting from interference patterns of all the individual resonances. The FFT, as a linear non-parametric processor, can give only the envelope or total shape spectra [2]. In contrast, the FPT as a non-linear parametric estimator, can generate the component as well as the total shape spectra [2]. This occurs because prior to constructing any spectrum, the FPT can retrieve the peak positions, widths, heights and phases of individual physical resonances.

The main distinction between these two kinds of processors is in the type of information extracted from the input time signal. Non-parametric processors can generate only qualitative information, which is used to plot graphs of spectral shapes. However, the quantitative data of critical importance are provided by parametric estimators through unfolding the hidden spectral structure of the envelope. The quantitative features of resonances (peak position, width, height and phase) reconstructed by the FPT are needed to estimate molecular concentrations. To re-emphasize, with the FPT, these key resonance parameters are retrieved first. Thereafter, the spectra can be constructed in any mode, if desired. This is a completely different methodology from fitting estimators that require the envelope spectrum from the FFT before attempting to quantify the encoded time signals. These two distinct approaches, the FFT followed by ambiguous fittings versus unambiguous and self-contained estimation by the FPT are anticipated to give substantially different results, especially with respect to closely overlapping resonances that are often of critical importance in applications across interdisciplinary fields, including atomic and molecular spectroscopy [18, 19].

The FPT converges when all the reconstructed genuine frequencies and amplitudes become stable. This point of stabilization is a veritable signature of recovery of the exact number K_G of genuine resonances ($K_G < K$). With any further increase of the partial signal towards the full signal length i.e. beyond the point at which full convergence was first reached, all the genuine frequencies and amplitudes remain constant and so do the ensuing spectra via the saturation $P_K/Q_K = P_{K_G+K_F}/Q_{K_G+K_F} = P_{K_G}/Q_{K_G}$, where K_F is the number of Froissart or spurious resonances. Protection against contamination by some K_F noisy or noise-like resonances is provided within the FPT itself, since each pole in the spectrum P_K/Q_K from spurious resonances stemming from the characteristic equation of the denominator polynomial $Q_K = 0$ coincides with the corresponding zero of the numerator polynomial, $P_K = 0$. This leads to pole-zero cancellation in the Padé polynomial quotient of the FPT. Such a feature can be used to differentiate between spurious and genuine content of the signal. Since the unphysical poles and zeros always appear as pairs in the FPT, they are viewed as doublets. These are called Froissart doublets after Froissart who, through numerical experiments, discovered this extremely useful phenomenon, which is unique to the Padé methodology [20, 21].

As a complement to our earlier studies [15]–[17] with the main focus of estimation of lineshapes in signal processing, the present study illustrates the use of the parametric version of the fast Padé transform in the theory of resonances. Our primary goal is to carry out a stringent testing of the FPT by verifying the possibility of obtaining the numerically exact solution of a highly challenging harmonic inversion problem with 25 tightly packed resonances, some of which are practically degenerate. Each resonance is characterized by four real parameters describing the spectral position, height, width and phase. Therefore, the present model signal possesses 100 real-valued spectral parameters. All these parameters have been entered into the analysis with 12 digit accuracy. Once the time signal is constructed as a linear combination of 25 damped complex harmonics and digitized, the input data for solving the quantification problem consists merely of the numerical values of the signal points. The task is to retrieve all the 12-digit accurate 100 input spectral parameters together with the exact number K_G of genuine resonances. This would expose the fast Padé transform to the most challenging testing for stability and robustness against perturbations due to the unavoidable computational round-off errors. Spectral analyzers that do not pass such a demanding and fully controlled testing cannot be considered as reliable when dealing with the corresponding experimentally measured time signals.

2 Theory

By way of a clear introduction to the FPT, we shall briefly recall the major features of rational functions. General rational functions $R(z^{-1})$ are defined as quotients of two other functions $f(z^{-1})$ and $g(z^{-1})$:

$$R(z^{-1}) = \frac{f(z^{-1})}{g(z^{-1})}. \quad (2.1)$$

Here, for convenience, the independent variable z^{-1} is chosen as the inverse of a general complex variable z . These rational functions represent the leading class of functions from mathematics with a myriad of applications across interdisciplinary research fields, ranging from physics to life sciences. This is primarily due to the main features of rational approximations, as they apply to analysis and interpretation of data that can stem from either experimental measurements or from theory by means of numerical computations. Such features are interpolation and extrapolation. By interpolation, one attempts to reliably generate the values of the observables in certain ranges or points where measured data are unavailable. By extrapolation, one tries to faithfully predict the values that could have been measured had the experiment continued beyond the last recorded data point of the studied physical quantity. Both cases are of great practical importance, since a reliable method would save extra measurements or time consuming numerical computations. Yet, the goal of an optimal theory is not to try in vain to achieve physically adequate interpolation and extrapolation by fitting with unavoidable non-uniqueness, subjectivity and bias. Rather, the aim is to ingrain these two features into adequate mathematical models without adjustable parameters for the purpose of description of measured phenomena. The most suitable framework for solving this challenging simultaneous interpolation-extrapolation problem is provided precisely by rational functions of the general type (2.1). Interpolation and extrapolation are also inherent in the important problem of sequence-to-sequence transformations as well as resummations of asymptotic and divergent series and sequences [13, 14]. In Ref. [2] a detailed analysis has been reported on the relationships of the FPT with a number of the well-known transforms due to Aitken, Shanks, Wynn, Levin, etc. In particular, the Levin transforms and several more modern related methods [13, 14] could advantageously be applied to spectral analysis from the present work.

The simplest, and crucially, the most powerful rational function, is the Padé approximant (PA), $R^{(\text{PA})}(z^{-1})$, which is introduced by a ratio of two polynomials $P_L^-(z^{-1})$ and $Q_K^-(z^{-1})$ of degrees L and K [2]:

$$R^{(\text{PA})}(z^{-1}) = \frac{P_L^-(z^{-1})}{Q_K^-(z^{-1})}, \quad (2.2)$$

$$P_L^-(z^{-1}) = \sum_{r=0}^L p_r^- z^{-r} \quad ; \quad Q_K^-(z^{-1}) = \sum_{s=0}^K q_s^- z^{-s}, \quad (2.3)$$

where $\{p_r^-, q_s^-\}$ are the expansion coefficients of $P_L^-(z^{-1})$ and $Q_K^-(z^{-1})$. The most stable are the diagonal and para-diagonal PA as obtained for $L = K$ and $L - 1 = K$, respectively. The polynomial ratio from (2.2) becomes unique if it is taken to approximate a given Maclaurin series $G(z^{-1})$ via $G(z^{-1}) \approx P_L^-(z^{-1})/Q_K^-(z^{-1})$ where:

$$G(z^{-1}) = \sum_{n=0}^{\infty} c_n z^{-n}. \quad (2.4)$$

In physics, the conventional Green function or the response function (spectrum) is also given by the expansion (2.4). In (2.4), the elements c_n of the infinite assembly $\{c_n\}$ are the known expansion coefficients that can be any set of numbers and not only time signal points. In applications to signal processing, the c_n 's from (2.4) are time signal points or auto-correlation functions [2]. These are given by linear combinations of decaying trigonometric functions that are complex-valued damped exponentials called fundamental harmonics (transients):

$$c_n = \sum_{k=0}^K d_k z_k^n \quad ; \quad z_k = e^{i\omega_k \tau} \quad , \quad \text{Im}(\omega_k) > 0. \quad (2.5)$$

Here, τ is the sampling or dwell time, whereas $\{\omega_k, d_k\}$ are the nodal angular frequencies and the associated amplitudes, respectively. By inserting (2.5) into $G(z^{-1})$ from (2.4), the infinite sum over n can be carried out using the exact result for the geometric series $\sum_{n=0}^{\infty} (z_k/z)^{-n} = 1/(1 - z_k/z) = z/(z - z_k)$. The obtained fraction $z/(z - z_k)$ is the simplest 1st order diagonal ($L = K = 1$) rational polynomial in the variable $z^{+1} \equiv z$. To cohere with (2.5), general variable z can also be written in the harmonic form $z = \exp(i\omega\tau)$, where ω is a running complex angular frequency. A sum of K fractions $z/(z - z_k)$ via $G(z^{-1}) = \sum_{n=0}^{\infty} c_n z^{-n} = \sum_{k=1}^K d_k \sum_{n=0}^{\infty} (z_k/z)^n = \sum_{k=1}^K z d_k / (z - z_k)$ represents the K th order diagonal ($L = K$) rational polynomial $P_K^+(z)/Q_K^+(z)$:

$$G(z^{-1}) = \sum_{k=1}^K \frac{z d_k}{z - z_k} \equiv \frac{P_K^+(z)}{Q_K^+(z)}, \quad (2.6)$$

$$P_L^+(z) = \sum_{r=1}^L p_r^+ z^r \quad , \quad Q_K^+(z) = \sum_{s=0}^K q_s^+ z^s. \quad (2.7)$$

Thus, for the expansion coefficients $\{c_n\}$ in the form of geometric progression (2.5), the exact result for the infinite sum in (2.4) is given precisely by the rhs of (2.6), which can alternatively be re-written as:

$$G(z^{-1}) \approx R^{(\text{PzT})}(z) \quad , \quad R^{(\text{PzT})}(z) \equiv \frac{P_K^+(z)}{Q_K^+(z)}. \quad (2.8)$$

Here, the acronym PzT stands for the so-called Padé z -transform. Distinguishing PA from PzT is essential due to the subtle, but critical differences (i) and (ii) between these two methods:

(i) The standard Padé approximant is invariably introduced in the literature on this method as the rational polynomial $P_L^-(z^{-1})/Q_K^-(z^{-1})$ from (2.2) in the same variable z^{-1} as the original function $G(z^{-1})$ from (2.4). On the other hand, we can alternatively interpret (2.4) as the usual z -transform in variable z^{-1} [2]. As such, subsequently using geometric progression (2.5) for the c_n 's, the resulting rational function $R^{(\text{PzT})}(z) = P_K^+(z)/Q_K^+(z)$ from (2.8) becomes the exact Padé polynomial quotient, but in the new variable z relative to the z -transform, $G(z^{-1})$. Thus, given $G(z^{-1})$, the first key difference between the PA and PzT is that the former and the latter are defined in variables z^{-1} and z , respectively. Of course, since the PzT is also a rational polynomial, the PzT and PA both belong to the same family of Padé approximants, albeit with two different tasks. To specify these tasks, given (2.4), we can consider two regions $|z| > 1$ and $|z| < 1$ in the complex z -plane. For $|z| > 1$ and $|z| < 1$, the series $G(z^{-1})$ from (2.4) will converge (say, slowly) and diverge, respectively. Therefore, the rational polynomial $P_K^-(z^{-1})/Q_K^-(z^{-1})$ from the usual PA in the same variable z^{-1} with respect to $G(z^{-1})$ accelerates the already existing convergence of (2.4) for $|z| > 1$. For the opposite case $|z| < 1$, the input series (2.4) diverges. However, for the same case $|z| < 1$, the rational polynomial $P_K^+(z)/Q_K^+(z)$ from the standard PzT converges, as it is defined in terms of the variable z as opposed to z^{-1} from $G(z^{-1})$. In this way, by means of the Cauchy analytical continuation, the PzT effectively induces convergence into the originally divergent series $G(z^{-1})$ for $|z| < 1$. This is how the same Padé methodology can achieve two opposite

mappings via transforming divergent series into convergent ones, and converting slowly into faster converging series (hence acceleration) [2].

(ii) The numerator polynomial $P_K^-(z^{-1})$ in e.g. the diagonal PA generally possesses the free, constant expansion coefficient p_0^- , such that the sum over r in (2.3) can start from $r = 0$ via: $P_K^-(z^{-1}) = p_0^- + p_1^- z^{-1} + p_2^- z^{-2} + \dots + p_K^- z^{-K}$ where $p_0^- \neq 0$. However, by definition, the corresponding expansion coefficient p_0^+ of the numerator polynomial $P_K^+(z)$ in the diagonal PzT is zero. Hence, this time, the sum over r in (2.7) for $P_K^+(z)$ begins with $r = 1$ with no free, z -independent term, so that: $P_K^+(z) = p_1^+ z + p_2^+ z^2 + \dots + p_K^+ z^K$ with $p_0^+ = 0$.

The mentioned uniqueness of the PA for the given input Maclaurin series (2.4) presents a key feature of this method. In other words, the ambiguities encountered in other mathematical modelings are eliminated from the outset already at the level of the definition of the PA. Moreover, this definition contains its “figure of merit” by revealing how well the PA can really describe the function $G(z^{-1})$ to be approximated. More precisely, given the infinite sum $G(z^{-1})$ via (2.4), the key question to raise is about the best agreement between $R^{(\text{PA})}(z^{-1})$ from (2.2) and $G(z^{-1})$ from (2.4). This question can be easily answered by expanding $R^{(\text{PA})}(z^{-1})$ as an infinite sum in powers of z^{-1} around the point z_∞ located at infinity, $z = z_\infty \equiv \infty$. The result can be symbolically expressed by:

$$G(z^{-1}) - \frac{P_L^-(z^{-1})}{Q_K^-(z^{-1})} = \mathcal{O}^-(z^{-L-K-1}) \quad , \quad z \longrightarrow \infty, \quad (2.9)$$

where $\mathcal{O}^-(z^{-L-K-1})$ is the remainder of power series expansions around $z = z_\infty = \infty$. The function $\mathcal{O}^-(z^{-L-K-1})$, as an explicit error of the approximation $G(z^{-1}) \approx P_L^-(z^{-1})/Q_K^-(z^{-1})$, itself represents a power series with the expansion terms z^{-L-K-m} ($m = 1, 2, 3, \dots, \infty$). In other words, the mentioned “figure of merit” is explicitly given by the easily obtainable error term $\mathcal{O}^-(z^{-L-K-1})$, which is an infinite sum with higher-order expansion terms than those retained in the Maclaurin series for the polynomial quotient $P_L^-(z^{-1})/Q_K^-(z^{-1})$ from the PA. The possibility of being able to explicitly compute the difference term or the error via $\mathcal{O}^-(z^{-L-K-1})$ in the Padé estimate $G(z^{-1}) \approx P_L^-(z^{-1})/Q_K^-(z^{-1})$ is the basis of a robust error analysis within the PA. Padé approximants can be computed through many different numerical algorithms, including the most stable numerical computations via continued fractions. Moreover, unlike any other related method, for the known $G(z^{-1})$, both Padé polynomials $P_L^-(z^{-1})$ and $Q_K^-(z^{-1})$ in the PA can be extracted by purely analytical means in their simple and concise closed forms [2]. This represents the gold standard against which all the corresponding numerical algorithms should be benchmarked for their stability and robustness.

Outside mathematics, *per se*, theoretical physicists are most appreciative of the power and usefulness of the PA [13, 14], which they began to use more than half a century ago in many problems ranging from the Brillouin-Wigner perturbation series to divergent expansions in quantum chromodynamics in the theory of strong interactions of elementary particles [2, 4]. The reason for such a widespread usage of this method in theoretical physics is that, in fact, the most interesting and also the most important series expansions emanating from realistic problems are divergent. Other frequently encountered series, although convergent in principle, often converge so slowly that they become virtually impractical in exhaustive applications. Here, the PA comes to rescue the situation in both cases by (a) converting divergent into convergent series and by (b) accelerating slowly converging series. The reason that the same method is able to tackle these diametrically opposite tasks (analytical continuations and convergence accelerations) is in the non-linearity of the PA, as is obvious from the definition (2.9).

The two main features of the Padé functions via its two wings, the PA (convergence rate enhancement of slowly convergent series or sequences), and the PzT (forced or induced convergence of originally divergent series) are jointly embodied into the fast Padé transform, the FPT. In the fast Padé transform, the PzT and PA are relabeled as $\text{FPT}^{(+)}$ and $\text{FPT}^{(-)}$, respectively, where the superscripts \pm refer to the employed independent variables, $z^{+1} \equiv z$ and $z^{-1} = 1/z$. By definition, the $\text{FPT}^{(+)}$ accomplishes analytical continuation through the forced convergence of divergent series. Likewise, the $\text{FPT}^{(-)}$ achieves acceleration of slowly converging series or sequences. Given a Maclaurin series (2.4), the $\text{FPT}^{(+)}$ and $\text{FPT}^{(-)}$ are aimed at approximating the same function $G(z^{-1})$:

$$G(z^{-1}) \approx R^{(\text{FPT})\pm}(z^{\pm 1}). \quad (2.10)$$

Functions $R^{(\text{FPT})\pm}(z^{\pm 1})$ are explicitly defined as rational polynomials:

$$R^{(\text{FPT})\pm}(z^{\pm 1}) \equiv \frac{P_L^\pm(z^{\pm 1})}{Q_K^\pm(z^{\pm 1})}, \quad (2.11)$$

$$P_L^\pm(z^{\pm 1}) = \sum_{r=1,0}^L p_r^\pm z^{\pm r} \quad , \quad Q_K^\pm(z^{\pm 1}) = \sum_{s=0}^K q_s^\pm z^{\pm s}, \quad (2.12)$$

where $r = 0$ and $r = 1$ correspond to $P_L^-(z^{-1})$ and $P_L^+(z)$, respectively. As in (2.9), the quality of the $\text{FPT}^{(+)}$ i.e. the adequacy of the two approximations in (2.10), is governed by the explicit definition:

$$G(z^{-1}) - \frac{P_L^+(z)}{Q_K^+(z)} = \mathcal{O}(z^{L+K+1}) \quad , \quad z \longrightarrow 0. \quad (2.13)$$

The remainders or error functions $\mathcal{O}^\pm(z^{\pm(L+K+1)})$ follow by developing $R^{(\text{FPT})^\pm}(z^{\pm 1})$ in their power series. Such developments imply that both rational functions $P_L^\pm(z^{\pm 1})/Q_K^\pm(z^{\pm 1})$ are able to exactly reproduce the first $L+K$ terms from the infinite set $\{c_n\}$ of the input Maclaurin series (2.10). By definition, the rational polynomials $P_L^+(z)/Q_K^+(z)$ and $P_L^-(z^{-1})/Q_K^-(z^{-1})$ from the $\text{FPT}^{(+)}$ and $\text{FPT}^{(-)}$ yield the series expansions in powers of z and $1/z$. Therefore, the remainders $\mathcal{O}(z^{L+K+1})$ and $\mathcal{O}(z^{-L-K-1})$ from (2.9) (2.13) are themselves power series expansions around the points $z = 0$ and $z = \infty$. When z is a harmonic variable as in MRS, where $z = \exp(i\omega\tau)$ and $\text{Re}(\omega) > 0$, then the $\text{FPT}^{(+)}$ and $\text{FPT}^{(-)}$ converge inside and outside the unit circle $|z| < 1$ and $|z| > 1$, respectively. However, being in the family of Padé approximants, the $\text{FPT}^{(+)}$ and $\text{FPT}^{(-)}$ (just like the PzT and PA) converge, as well, in the complementary regions $|z| > 1$ and $|z| < 1$, respectively, by virtue of their analytical continuations. In other words, the $\text{FPT}^{(\pm)}$ are defined throughout the complex z -plane with the exception of K poles $z = z_k^\pm$ ($1 \leq k \leq K$) of $P_K^\pm(z^{\pm 1})/Q_K^\pm(z^{\pm 1})$, where z_k^\pm are zeros of the denominator polynomials, $Q_K^\pm(z_k^\pm) = 0$. Once the K solutions $\{z_k^\pm\}$ of this latter characteristic or secular equations are available, the corresponding complex frequencies and amplitudes are extracted from the formulae: $\nu_k^\pm = \mp(i/\tau) \ln(z_k^\pm)$ and $d_k^\pm = P_K^\pm(z_k^\pm)/Q_K^{\pm'}(z_k^\pm)$, where $Q_K^{\pm'}(z^{\pm 1}) = (d/dz^{\pm 1})Q_K^\pm(z^{\pm 1})$ and $Q_K^{\pm'}(z_k^\pm) \neq 0$. These expressions for the amplitudes d_k^\pm are obtained by taking the Cauchy residues of the Padé polynomial quotients $P_K^\pm(z_k^\pm)/Q_K^\pm(z_k^\pm)$ evaluated at the poles $z^{\pm 1} = z_k^\pm$.

The above outlines emphasize the universal importance of rational functions and their most powerful proponent – Padé approximants. This led to a straightforward identification of the origin of the fast Padé transforms, via the $\text{FPT}^{(-)}$ and $\text{FPT}^{(+)}$, as the standard PA (acceleration of slowly converging series) and the PzT (transformation of diverging into converging series), respectively. However, in addition to convergence acceleration and induced convergence, the FPT can be applied to signal processing, where the main task is to carry out spectral analysis i.e. to solve the quantification problem. In this latter research area, a sampled time signal $\{c_n\}$ is available either from computations or measurements. Particularly in MRS, magnetic resonance physics dictates that each c_n is indeed a sum of K complex damped exponentials, as in (2.5). Here, we are given a set of N sampled time signal points $\{c_n\}$ ($0 \leq n \leq N-1$), where the dwell time τ and the total signal length N are also known. As stated, the principal goal in parametric signal processing is to solve the quantification problem as an inverse problem. For the input data $\{c_n\}$ ($0 \leq n \leq N-1$), as well as N and τ , this inverse problem amounts to finding the unique solutions for the three types of unknown quantities that are the complex fundamental frequencies $\{\omega_k\}$ and the corresponding complex amplitudes $\{d_k\}$, as the building elements of each c_n . Moreover, in this quantification problem, there is yet another unknown quantity and that is the number K_G of genuine resonances with the spectral parameters $\{\omega_k, d_k\}$ ($1 \leq k \leq K_G$).

A critically important feature of the FPT is its ability to reconstruct exactly the total true number of physical harmonics in the given FID. In practice, determination of the exact number of resonances can be accomplished via Froissart doublets [20] or pole-zero cancellations. The total number of genuine resonances is given by the degree K of the denominator polynomials Q_K^\pm . The only known information about this degree K is that it must obey the inequality $2K \leq N$. Algebraically, the $2K$ unknown spectral parameters (frequencies and amplitudes) require at least $2K$ signal points from the whole set of N available entries. To determine K unequivocally in non-parametric signal processing, we compute a short sequence of the FPTs by varying the degree K' of the polynomials in the Padé spectra $\{P_{K'}^\pm/Q_{K'}^\pm\}$ until all the ensuing results stabilize/saturate. When this happens, say at $K' = K''$, we are certain that the true number K is obtained as $K = K''$. If we continue on increasing the running order K' of the FPT beyond the stabilized value K , we would always obtain the same results for $K' = K + m$ and for K using any positive integer m . The mechanism by which this is achieved (i.e. the maintenance of the overall stability, including the constancy of the value of the true number of resonances) is provided by the concept of Froissart doublets [20].

Specifically, by not knowing the exact number K in advance, one would systematically augment the order $K' = K + m$ ($m = 1, 2, 3, \dots$) and this would lead to extra zeros from P_{K+m}^\pm and Q_{K+m}^\pm . All the solutions of the characteristic equations $P_{K+m}^\pm = 0$ and $Q_{K+m}^\pm = 0$ are the respective zeros and poles in the spectra P_{K+m}^\pm/Q_{K+m}^\pm because these latter rational polynomials are meromorphic functions (functions whose only singularities are poles are meromorphic functions). Such extra zeros and poles are spurious, since they are not a part of the input FID, which is built from the K true harmonics alone. These spurious poles and zeros coincide with each other. Therefore, in the spectra P_{K+m}^\pm/Q_{K+m}^\pm , beyond the stabilized number K of resonances, all the spurious poles and zeros will be automatically

Table 1. Twelve digit numerical values for all the input spectral parameters: the real $\text{Re}(\nu_k)$ and the imaginary $\text{Im}(\nu_k)$ part of complex frequencies ν_k , and the absolute values $|d_k|$ of amplitudes d_k of 25 damped complex exponentials from the synthesized time signal (2.5) similar to a short echo time (~ 20 ms) encoded FID via MRS at the magnetic field strength $B_0=1.5$ T from a healthy human brain, as in Ref. [22]. Every phase $\{\phi_k\}$ of the amplitudes is equal to zero, such that each d_k is purely real, $d_k = |d_k|\exp(i\phi_k) = |d_k|$.

INPUT DATA for ALL SPECTRAL PARAMETERS of a SYNTHESIZED TIME SIGNAL or FID

n_k°	$\text{Re}(\nu_k)$ (ppm)	$\text{Im}(\nu_k)$ (ppm)	$ d_k $ (au)	M_k
1	0.98501398674	0.18001465258	0.12203235945	Mob. Lip
2	1.11203168723	0.25701463975	0.16102534769	Mob. Lip
3	1.54802256874	0.17202754365	0.13502234563	Mob. Lip
4	1.68903478456	0.11803476587	0.03401524874	Mob. Lip
5	1.95901375986	0.06203746798	0.05602324897	Gaba
6	2.06502285659	0.03101654587	0.17102458679	NAA
7	2.14501198543	0.05002471356	0.11603534867	NAAG
8	2.26102368757	0.06203456897	0.09201183765	Gaba
9	2.41103487259	0.06202653745	0.08502419328	Glu
10	2.51902265397	0.03601654189	0.03703346957	Gln
11	2.67601285971	0.03302569432	0.00803438479	Asp
12	2.67601285972	0.06201675478	0.06301243246	NAA
13	2.85503367438	0.01603187452	0.00502167879	Asp
14	3.00902483679	0.06401569438	0.06503534245	Cr
15	3.06701235896	0.03602786435	0.10102493987	PCr
16	3.23903157914	0.05003467587	0.09601373648	Cho
17	3.30101296785	0.06402537896	0.06501124867	PCho
18	3.48102497584	0.03103548627	0.01102547368	Tau
19	3.58401351765	0.02801457683	0.03603282549	m-Ins
20	3.69402268739	0.03602617584	0.04102389436	Glu
21	3.80303157594	0.02401584975	0.03101432657	Gln
22	3.94402312958	0.04203725359	0.06803345832	Cr
23	3.96503247623	0.06202681945	0.01302532687	PCr
24	4.27101432576	0.05503473576	0.01603293478	PCho
25	4.68000000000	0.12201256293	0.08501458765	Water

canceled due to the quotient form of the Padé spectra, so that:

$$\frac{P_{K+m}^\pm}{Q_{K+m}^\pm} = \frac{P_K^\pm}{Q_K^\pm} \quad (m = 1, 2, 3, \dots). \quad (2.14)$$

Hence stability of the Padé spectral estimation. This stabilization condition is the signature of the determination of the exact total number K of resonances. If the quantification problem is solved first, then the subsequent stability via (2.14) will stem from the constancy of all the spectral parameters that are reconstructed exactly by the FPT from the given FID. Of course, once all the parameters are reconstructed, it is not mandatory to search for saturation (2.14) in the corresponding spectra from the FPT. In such a parametric signal processing within the FPT, the exact number K of genuine resonances is determined by monitoring solely the potential constancy of all the found spectral parameters. In this way, one may say that irrespective of whether poles or zeros are explicitly available or not, the stabilization principle implicitly act by effectively reducing P_{K+m}^\pm/Q_{K+m}^\pm to P_K^\pm/Q_K^\pm , as per (2.14). Such a lowering of the degrees of the characteristic polynomials from $K + m$ to K , with parametric *and* non-parametric estimations within the FPT^(±) promotes the stabilization concept to the status of an efficient method for reduction of the original dimensionality of the problem. Note that the problem of dimensionality reduction in itself is a very important issue in the field of system theory, especially when dealing with large degrees of freedom [2]. Large systems are difficult to handle in any computation and, therefore, it is essential to reduce their original dimension without any information loss. This is important even without the obvious concern for computational demands because capturing the essence of the investigated large system by an adequate extraction of a relatively small number of the main parametrizing characteristics allows simple and yet reliable descriptions. To achieve this goal, the parametric version of the FPT does not need a specially designed procedure, since stabilization of spectra and spectral parameters solve the dimensionality reduction problem while separating genuine from spurious information.

3 Results

We use (2.5) to generate a complex-valued synthesized time signal $\{c_n\}$ ($0 \leq n \leq N - 1$), which is also called the free induction decay (FID) curve. The chosen signal length N is $N = 1024$ and the bandwidth is set to be 1000 Hz. This yields the sampling rate $\tau = 1$ ms and the total duration time of the signal $T = N\tau = 1.024$ s. Table 1 gives the 12-digit input data for the quantification problem to be solved in the present work. These data are the complex fundamental frequencies and the corresponding amplitudes from the noise-free model signal (2.5) whose associated spectrum is comprised of a total of 25 resonances, some of which are individual although tightly packed peaks, while others are closely-overlapped or nearly degenerate. The numerical values of the spectral parameters were chosen to correspond to the typical frequencies and amplitudes found in proton MR time signals encoded *in vivo* from healthy human brain at 1.5T [22]. The columns in Table 1 of the input fundamental transients are headed by labels n_k° , $\text{Re}(\nu_k)$ (ppm), $\text{Im}(\nu_k)$ (ppm), $|d_k|$ (au) and M_k that represent the running number, real and imaginary frequencies (both in parts per million, ppm), absolute values of amplitudes (in arbitrary units, au) and the molecular (metabolite) assignments, respectively. The phases of all the amplitudes are set to be equal to zeros. Of particular note are the crossings of the 2nd column with the 11th and 12th rows where the two chemical shifts $\text{Re}(\nu_{11}) = 2.67602157683$ ppm and $\text{Re}(\nu_{12}) = 2.67602157684$ ppm are separated by an exceedingly small splitting $\text{Re}(\nu_{12}) - \text{Re}(\nu_{11}) = 1 \times 10^{-11}$ ppm.

The results of the $\text{FPT}^{(-)}$ for machine accurate exact reconstructions of the input spectral parameters are given in Table 2. It can be seen that a varying level of accuracy is attained in the retrieved spectral parameters from the $\text{FPT}^{(-)}$ near full convergence at 2 partial signal lengths $N_P = 180, 220$. Neither length is compliant with the FFT-type lengths i.e. we have $N_P \neq 2^m$ (m positive integers). On panel (i) at $N_P = 180$, before full convergence is achieved, some 2 – 7 reconstructed digits can be seen. Note that the 11th resonance is not detected here. Its absence is marked by the sign “–” in the first column at the corresponding vacant location ($n_k^\circ = 11$). However, at $N_P = 220$ an enormous increase in accuracy is observed on panel (ii), with all the 12 input digits exactly reconstructed for each spectral parameter of 25 resonances. The phases of the amplitudes are not displayed, but they are also retrieved with 12 digit accuracy at $N_P = 220$. Remarkably, with only 220 signal points out of 1024 entries from the full FID, the $\text{FPT}^{(-)}$ resolves unequivocally the two near degenerate frequencies separated from each other by an unprecedented chemical shift of merely 10^{-11} ppm. This shows that the $\text{FPT}^{(-)}$ has an exponential convergence rate (the spectral convergence) to the exact numerical values within machine accuracy of all the reconstructed fundamental frequencies and the associated amplitudes. Moreover, these 12-digit output results for the 12-digit input data prove an indeed unprecedented robustness of the $\text{FPT}^{(-)}$ even against computational round-off-errors.

All the remaining computations will be illustrated graphically in Figs. 1–7 and, for this purpose, it is sufficient to use only the first three decimals from the input data in Table 1. In such a case, the chemical shifts for the resonances with $n_k^\circ = 11$ and $n_k^\circ = 12$ would be identical, and to avoid the exact degeneracy, we shall make the redefinitions $\text{Re}(\nu_{11}) = 2.675$ ppm and $\text{Re}(\nu_{12}) = 2.676$. Figure 1 shows, on panels (i) and (ii), the real $\text{Re}(c_n)$ and imaginary $\text{Im}(c_n)$ part of the synthesized FID. Panel (iii) in this figure displays the initial convergence regions of the $\text{FPT}^{(+)}$ and $\text{FPT}^{(-)}$ located inside and outside the unit circle $|z| < 1$ and $|z| > 1$ in the complex planes of the harmonic variables z and z^{-1} , respectively. Since the Padé spectra are rational functions given by the quotients of two polynomials, the Cauchy analytical continuation principle lifts the restrictions of the initial convergence regions. Namely, the Cauchy principle extends the initial convergence region from $|z| < 1$ to $|z| > 1$ for the $\text{FPT}^{(+)}$ and similarly from $|z| > 1$ to $|z| < 1$ for the $\text{FPT}^{(-)}$. Thus, both the $\text{FPT}^{(+)}$ and $\text{FPT}^{(-)}$ continue to be computable throughout the complex frequency plane without encountering any divergent regions. An exception is the set of the fundamental frequencies of the examined FID that are simultaneously the singular points (poles) of the system’s response function. The small dots seen on panel (iii) depict both the exact input harmonic variables $z_k^{\pm 1} = \exp(\pm i\omega_k\tau)$ and the corresponding Padé counterparts $z_k^{\pm} = \exp(\pm i\omega_k^{\pm}\tau)$ reconstructed with $N/4 = 256$ where $\omega_k = 2\pi\nu_k$ and $\omega_k^{\pm} = 2\pi\nu_k^{\pm}$. On panel (iii) the locations of the 1st and the 25th damped harmonics for lipid and water are denoted by Lip and H₂O, respectively. These represent the two endpoints of the complex harmonic variable interval within which all the 25 studied resonances reside. To avoid clutter, numbers for the remaining 23 resonances on both sides of the circumference $|z| = 1$ are not written on panel (iii). These numbers will be shown in Figs. 4 and 5, whereas the corresponding acronyms for the metabolites shall be depicted in Fig. 3. Panels (iv) and (v) in Fig. 1 display the two Padé absorption total shape spectra from the Heaviside partial fractions of the $\text{FPT}^{(+)}$ and $\text{FPT}^{(-)}$, respectively, computed using a quarter signal length ($N/4 = 256$). These results are identical to those obtained with $N/2 = 512$ and $N = 1024$. Panel (vi) in Fig. 1 presents the Fourier absorption total shape spectrum evaluated via the FFT using the full FID with $N = 1024$. A comparison of panels (iv)–(vi) in Fig. 1 reveals that zero-valued spectra are obtained from the difference between any two selected pairs of these spectra.

In Fig. 2 we present the absorption total shape spectra computed by the FFT (left column) and $\text{FPT}^{(-)}$ (right column) at three partial signal lengths. On panels (i) and (iv) in Fig. 2, the most dramatic difference between the FFT and $\text{FPT}^{(-)}$ is seen at the shortest signal length ($N/8 = 128$). Here, the FFT essentially presents little meaningful

Table 2. Two to twelve digit accuracy for the complex frequencies and amplitudes reconstructed by the $\text{FPT}^{(-)}$ at partial signal lengths $N_P = 180$ and 220 . Notice, especially, that using only 220 signal points out of 1024 entries available from the full FID, the $\text{FPT}^{(-)}$ resolves unequivocally the two near degenerate frequencies separated from each other by an unprecedented chemical shift of merely 10^{-11} ppm.

PROOF-OF-PRINCIPLE ACCURACY of $\text{FPT}^{(-)}$ for QUANTIFICATION ; FID LENGTHS: $N_P = 180, 220$

Accuracy of $\text{FPT}^{(-)}$ for every parameter of each resonance: 2 – 7 Exact Digits (ED_k^-)

n_k^o	$\text{Re}(v_k^-)$ (ppm)	ED_k^-	$\text{Im}(v_k^-)$ (ppm)	ED_k^-	$ d_k^- $ (au)	ED_k^-
1	0.9850237	5	0.1800194	5	0.1220619	4
2	1.1120512	4	0.2569843	4	0.1609715	4
3	1.5480096	5	0.1720104	5	0.1349519	4
4	1.6890928	4	0.1180372	6	0.0340191	6
5	1.9589440	4	0.0620274	5	0.0559128	4
6	2.0649981	4	0.0309978	5	0.1707346	4
7	2.1452547	4	0.0499006	4	0.1153643	3
8	2.2613642	4	0.0625697	3	0.0938521	3
9	2.4107820	3	0.0631962	3	0.0883812	3
10	2.5178233	3	0.0358176	4	0.0366389	4
–	–	–	–	–	–	–
12	2.6756914	4	0.0541871	2	0.0662096	2
13	2.8555552	3	0.0145382	3	0.0045096	4
14	3.0111369	3	0.0588950	3	0.0597010	2
15	3.0660880	3	0.0367181	3	0.1073692	2
16	3.2403693	3	0.0510559	3	0.1037399	2
17	3.2994204	3	0.0606733	3	0.0608598	2
18	3.4799613	3	0.0301651	3	0.0105043	3
19	3.5841217	4	0.0277123	4	0.0354333	3
20	3.6942698	4	0.0359785	4	0.0408703	4
21	3.8030803	4	0.0240617	4	0.0310847	4
22	3.9440911	4	0.0418756	4	0.0671497	3
23	3.9639891	2	0.0609991	3	0.0140652	3
24	4.2710137	7	0.0550357	6	0.0160335	6
25	4.6800001	7	0.1220122	6	0.0850142	6

(i) Partial FID Length: $N_P = 180$

Accuracy of $\text{FPT}^{(-)}$ for every parameter of each resonance: 12 Exact Digits (ED_k^-)

n_k^o	$\text{Re}(v_k^-)$ (ppm)	ED_k^-	$\text{Im}(v_k^-)$ (ppm)	ED_k^-	$ d_k^- $ (au)	ED_k^-
1	0.98501398674	12	0.18001465258	12	0.12203235945	12
2	1.11203168723	12	0.25701463975	12	0.16102534769	12
3	1.54802256874	12	0.17202754365	12	0.13502234563	12
4	1.68903478456	12	0.11803476587	12	0.03401524874	12
5	1.95901375986	12	0.06203746798	12	0.05602324897	12
6	2.06502285659	12	0.03101654587	12	0.17102458679	12
7	2.14501198543	12	0.05002471356	12	0.11603534867	12
8	2.26102368757	12	0.06203456897	12	0.09201183765	12
9	2.41103487259	12	0.06202653745	12	0.08502419328	12
10	2.51902265397	12	0.03601654189	12	0.03703346957	12
11	2.67601285971	12	0.03302569432	12	0.00803438479	12
12	2.67601285972	12	0.06201675478	12	0.06301243246	12
13	2.85503367438	12	0.01603187452	12	0.00502167879	12
14	3.00902483679	12	0.06401569438	12	0.06503534245	12
15	3.06701235896	12	0.03602786435	12	0.10102493987	12
16	3.23903157914	12	0.05003467587	12	0.09601373648	12
17	3.30101296785	12	0.06402537896	12	0.06501124867	12
18	3.48102497584	12	0.03103548627	12	0.01102547368	12
19	3.58401351765	12	0.02801457683	12	0.03603282549	12
20	3.69402268739	12	0.03602617584	12	0.04102389436	12
21	3.80303157594	12	0.02401584975	12	0.03101432657	12
22	3.94402312958	12	0.04203725359	12	0.06803345832	12
23	3.96503247623	12	0.06202681945	12	0.01302532687	12
24	4.27101432576	12	0.05503473576	12	0.01603293478	12
25	4.68000000000	12	0.12201256293	12	0.08501458765	12

(ii) Partial FID Length: $N_P = 220$

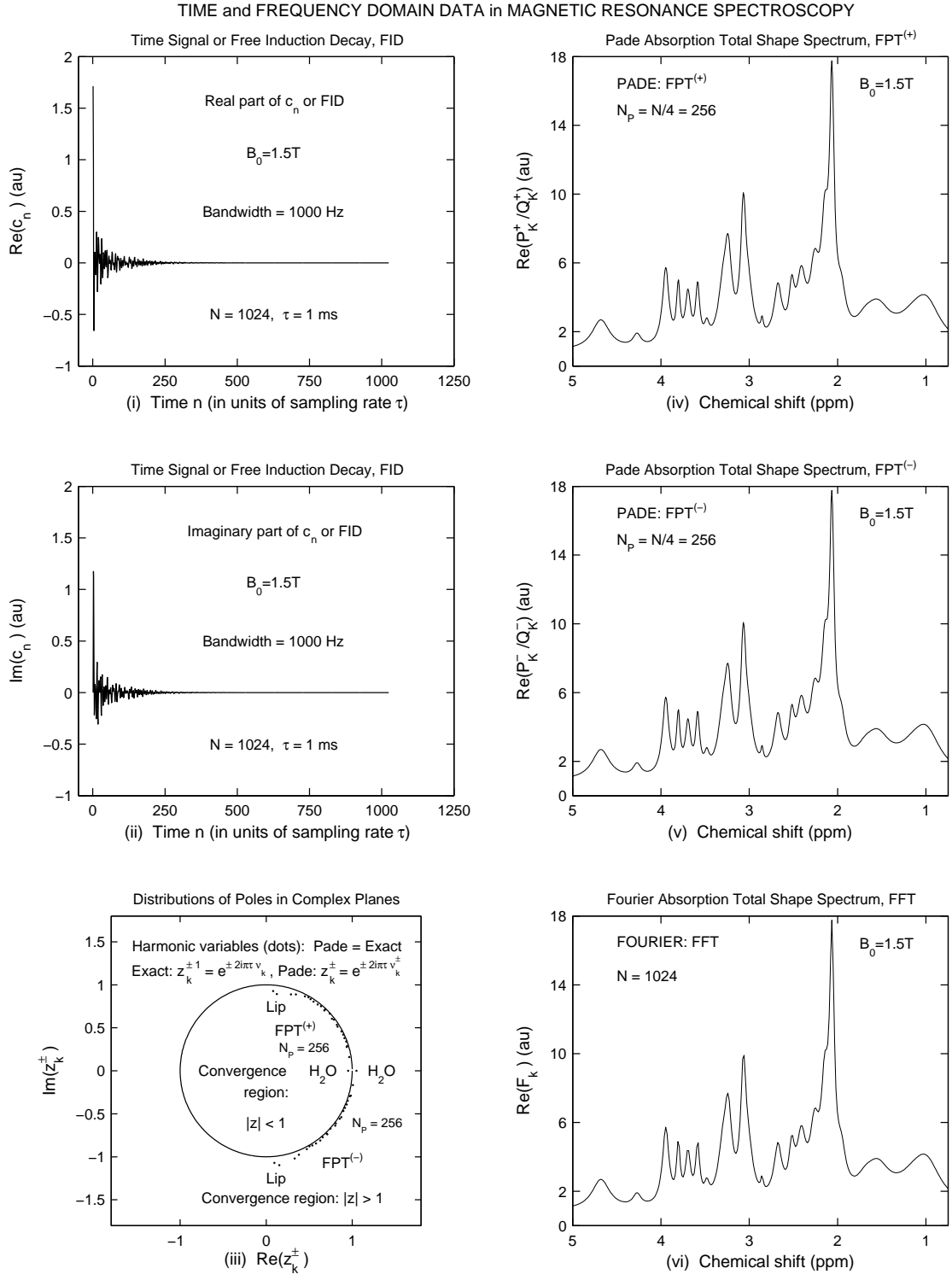


Figure 1: Time signal (panels (i), (ii)) and the corresponding absorption total shape spectra (envelope) in the FPT^{\pm} (panels (iv), (v)) and FFT (panel (vi)). The initial convergence regions in the $\text{FPT}^{(+)}$ and $\text{FPT}^{(-)}$, inside and outside the unit circle, respectively, are shown on panel (iii).

spectroscopic information. In contrast, with the $\text{FPT}^{(-)}$, at $N/8 = 128$, several major peaks are clearly delineated, such as NAA, Cre, Cho, etc. On panel (ii) at $N/4 = 256$, the FFT has still not predicted the correct height of even the largest resonance (NAA) around 2 ppm and, simultaneously, a number of other peaks are unresolved. On the other hand, with the $\text{FPT}^{(-)}$ shown on panel (iv) at $N/4 = 256$, full convergence of the total shape spectrum is reached. At half signal length $N/2 = 512$ on panel (iii), the height of the NAA peak in the FFT is still too short, thus causing the lack of convergence for the whole Fourier spectrum. However, on panel (vi) at $N/2 = 512$, the $\text{FPT}^{(-)}$ maintains its complete convergence by way of pole-zero cancellations. Overall, it is seen from Fig. 2 that the $\text{FPT}^{(-)}$ converges faster than the FFT as the partial signal length is gradually augmented. Moreover, the $\text{FPT}^{(-)}$ produces no Gibbs ringing in the process of converging in a steady fashion as a function of the increased signal length. This is in sharp contrast to other existing parametric estimators that are usually unstable as a function of N_P , typically undergoing wide oscillations with unacceptable results before eventually converging, if they do at all.

Figure 3 compares the results for the $\text{FPT}^{(+)}$ and $\text{FPT}^{(-)}$ (left and right columns). The pertinent details with regard to panels (i) and (iv) as well as (ii) and (v) of Fig. 3 have already been presented in section Fig. 1. Nevertheless, further important information is presented on panels (ii) and (v) in Fig. 3 for the absorption total shape spectra by displaying the usual acronyms that locate the positions of the major MR-detectable metabolites associated with resonances stemming from FIDs encoded via MRS from a healthy human brain. Here, the same acronyms for several resonances (Cho, Glu, NAA) are seen at more than one chemical shift. This is a consequence of the so-called J-coupling [1]. On panels (iii) and (vi) in Fig. 3, the absorption component shape spectra are presented for each individual resonance. The sums of all of such component shape spectra yield the associated total shape spectra from panels (ii) and (v) in Fig. 3. Once again it is seen on panels (iii) and (vi) in Fig. 3, that only a quarter $N/4 = 256$ of the full FID is necessary for both the $\text{FPT}^{(+)}$ and $\text{FPT}^{(-)}$ to fully resolve all the individual resonances, including the peaks that are isolated ($n_k^\circ = 8, 9, 10, 13, 18, 19, 20, 21, 24, 25$), overlapped ($n_k^\circ = 1, 2; n_k^\circ = 3, 4; n_k^\circ = 5, 6, 7; n_k^\circ = 14, 15; n_k^\circ = 16, 17$), tightly overlapped ($n_k^\circ = 22, 23$) as well as nearly degenerate ($n_k^\circ = 11, 12$). Furthermore, panels (iii) and (vi) of this figure show that the component shape spectra coincide in the $\text{FPT}^{(+)}$ and $\text{FPT}^{(-)}$, as in Fig. 1. Such an equivalence of these two variants is due to the uniqueness of reconstructions in the fast Padé transform.

Figure 4 reveals further insights into the exact quantification within the $\text{FPT}^{(+)}$. As was previously the case in Figs. 1 and 3, all the obtained results are for $N/4 = 256$. The absorption total shape spectrum is shown on panel (iv) in Fig. 4, where the individual numbers of resonances are located near the related peaks. Thus each well-resolved isolated resonance is marked by the corresponding separate number e.g. $n_k^\circ = 8, 9$, etc. Similarly, the overlapped, tightly overlapped and nearly degenerate resonances are labeled as the sum of the pertinent peak numbers e.g. $n_k^\circ = 1 + 2$ or $n_k^\circ = 5 + 6 + 7$, etc. On panel (v) in Fig. 5, the absorption component shape spectra of the constituent resonances $n_k^\circ = 1 - 25$ are shown, and all the individual numbers are indicated for an easier comparison with panel (iv) on the same figure. Thereby, the hidden structures are well-delineated in these component shape spectra. These hidden resonances are those that are overlapped ($n_k^\circ = 1 + 2, 3 + 4, 5 + 6 + 7, 14 + 15, 16 + 17$), tightly overlapped ($n_k^\circ = 22 + 23$) and nearly degenerate ($n_k^\circ = 11 + 12$). As seen on panel (v), most resonances e.g. $n_k^\circ = 5 - 24$ are rather narrow as implied by the relatively small values of $\text{Im}(\nu_k^+)$. Thus, these imaginary frequencies are quite close to the real axis. As a result, these resonances are seen on panel (vi) in a group in the middle part of this sub-plot. In contrast, panel (vi) in Fig. 4 shows wider resonances e.g. $n_k^\circ = 1 - 4$ and $n_k^\circ = 25$ with larger values of $\text{Im}(\nu_k^+)$. Thus, such imaginary frequencies are deeper in the complex plane and these resonances are quite distant from the real axis, as observed on the far left and the far right parts of panel (vi). Besides panel (vi) in Fig. 4, graphic presentations of the reconstructed and the input data for the spectral parameters are also presented on panels (i) – (iii). Panel (i) in Fig. 4 depicts the distribution of the absolute values of the amplitudes at different chemical shifts. It follows from panel (i) that the quantities $|d_k^+|$ do not represent the heights of the absorption peaks from panels (iv) and (v). Instead, the absorption peak heights are directly proportional to the quotient $|d_k^+|/\text{Im}(\nu_k^+)$, as it should be with any Lorentzian. Thus in Fig. 4, panel (ii) displays the distribution of these latter quotients of the absolute values of the amplitudes and the imaginary frequencies. It can be observed from panel (ii) that all the 25 ratios $|d_k^+|/\text{Im}(\nu_k^+)$ are, in fact, proportional to the heights of the corresponding peaks in the absorption component shape spectra from panel (v) in Fig. 4. Panel (iii) from Fig. 4 shows, in the complex z^+ -plane, the distribution of the Padé poles using the complex harmonic variable z_k^+ . This is the zoomed version of panels (iii) or (i) from Figs. 1 or 3, respectively. The difference is in displaying only the first quadrant in Fig. 4, since the rest of the complex z^+ -plane does not contain any genuine resonance. Note that on panel (vi), both $\text{Re}(\nu_k^+)$ and $\text{Im}(\nu_k^+)$ are shown in descending order when proceeding from left to right on the abscissa or from bottom to top on the ordinate in Fig. 4. This convenient layout reveals that all the Padé poles $n_k^\circ = 1 - 25$ are aligned one after the other from right to left regarding the abscissa. The same poles $n_k^\circ = 1 - 25$ are also packed together near the circumference ($|z| = 1$) of the unit circle in such a way that they follow each other according to their consecutive numbers from inside the unit circle, by being aligned upward with respect to the ordinate, as per panel (iii). Panel (iii) in Fig. 4 shows that the poles contained in the harmonic variable

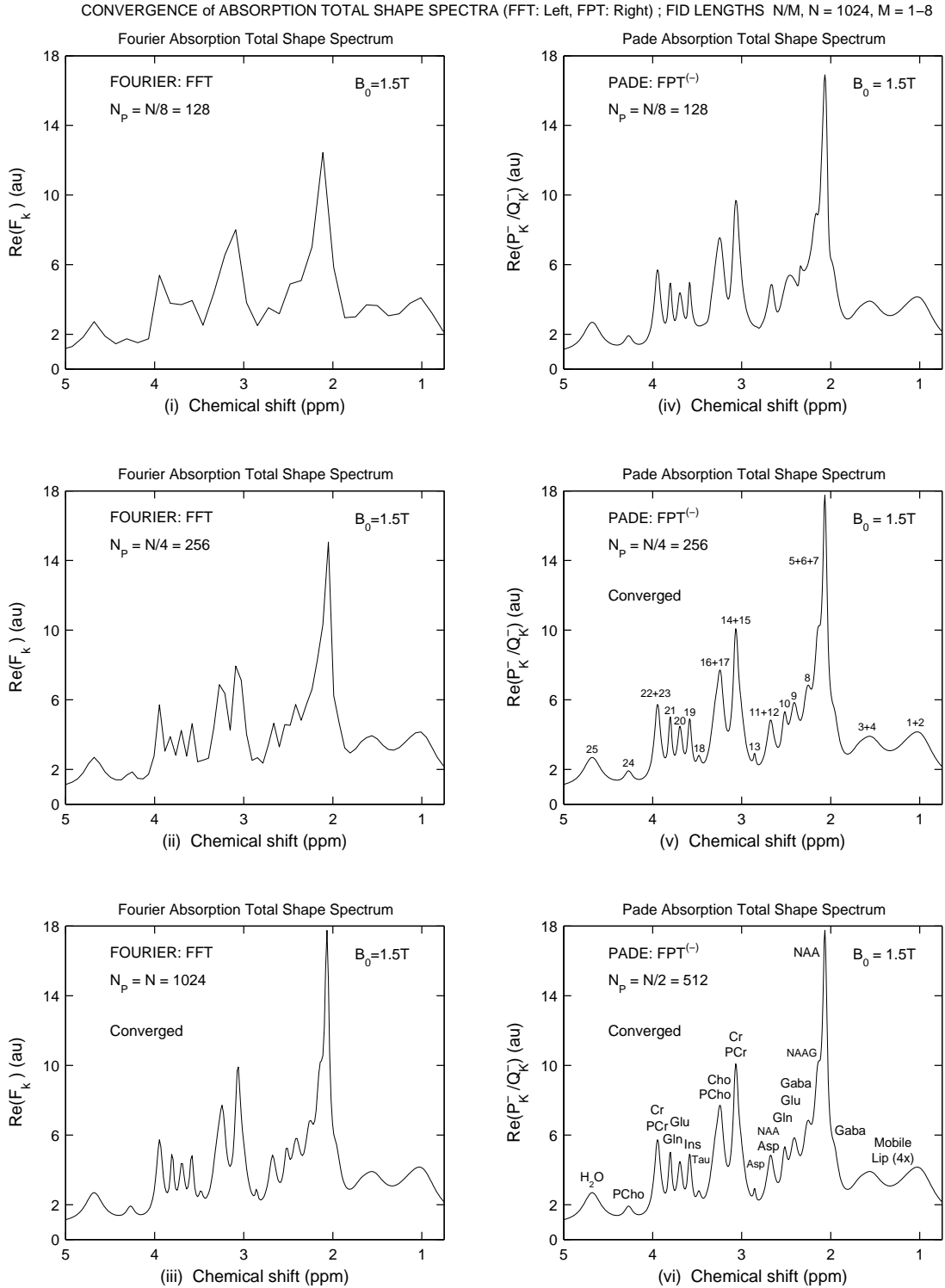


Figure 2: Convergence rate as a function of the partial signal length N_P at the fixed bandwidth, 1000 Hz. Fourier (FFT, left panel) and Padé (FPT⁽⁻⁾, right panel) absorption total shape spectra computed using the time signal from Fig. 1 at three different lengths $N/8 = 128$, $N/4 = 256$ and $N = 1024$ as displayed on the top, middle and bottom panels, respectively, where the full signal length is $N = 1024$.

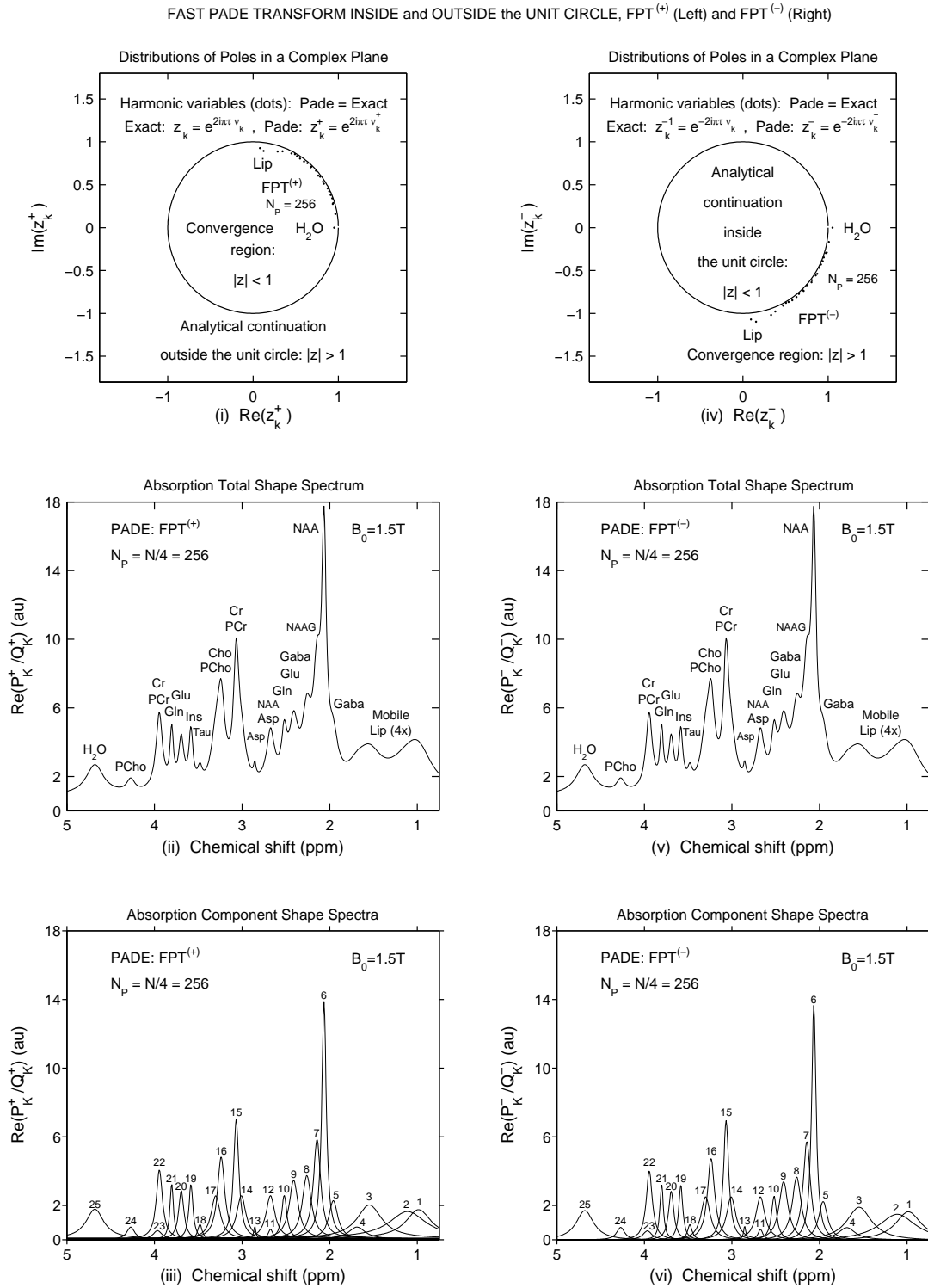


Figure 3: The initial convergence regions (panels (i), (iv)), absorption total shape spectra (panels (ii), (v)) and absorption component shape spectra (panels (iii), (vi)) in the $FPT^{(+)}$ (left column) and $FPT^{(-)}$ (right column). The middle panels display the usual acronyms for the main MR-detectable metabolites in the healthy human brain, whereas the bottom panels give the corresponding numbers of these metabolites (see Table 1).

z_k^+ in the polar coordinates are less scattered from each other relative to the associated distributions of the complex frequencies from panel (vi) in the rectangle Descartes coordinates. The reason for this is in the exponential function of the complex frequency which is plotted on panel (iii), whereas the frequency itself is shown on panel (vi) in Fig. 4. It is seen on panel (iii) in this figure that all the genuine poles retrieved by the $\text{FPT}^{(+)}$ are found inside the unit circle ($|z| < 1$), as expected. Notice that narrow resonances $n_k^\circ = 5 - 24$ are shown to be near the circumference ($|z| = 1$) of the unit circle. On the other hand, the wide resonances seen on panel (iii) in Fig. 4, such as $n_k^\circ = 1 - 4$ and $n_k^\circ = 25$, lie further from the borderline $|z| = 1$.

Figure 5 displays the results of the $\text{FPT}^{(-)}$. The interpretation of the results from the $\text{FPT}^{(+)}$ as presented on panels (i), (ii) and (iv) – (vi) in Fig. 4 holds as well with respect to the corresponding findings from the $\text{FPT}^{(-)}$ shown on panels (i), (ii) and (iv) – (vi) in Fig. 5. This observation emerges from the fact that the $\text{FPT}^{(+)}$ and $\text{FPT}^{(-)}$ generate indistinguishable spectral parameters for the same number of signal points, $N/4 = 256$. However, panel (iii) differs for Figs. 4 and 5, since the information presented in these plots relates to the two complementary regions of the initial convergence, inside and outside the unit circle, for the $\text{FPT}^{(+)}$ and $\text{FPT}^{(-)}$, respectively. In order to match the configuration from panel (iii) in Fig. 4, the Padé poles contained in the harmonic variable z_k^- , as displayed in the complex z^- – plane on panel (iii) in Fig. 5, are plotted with the values of $\text{Im}(z_k^-)$ in ascending order when going from bottom to top of the ordinate. This is opposite to the ordering of $\text{Im}(z_k^+)$ on panel (iii) in Fig. 4, as anticipated because $\text{Im}(z_k^+) > 0$ and $\text{Im}(z_k^-) < 0$. Thus, in reconstructions by the $\text{FPT}^{(+)}$ and $\text{FPT}^{(-)}$, the harmonic variables z_k^+ and z_k^- are located in the first and the fourth quadrant of the complex z^+ – and z^- – planes, respectively. This is apparent on panel (iii) of Fig. 1 or on panels (i) and (iv) in Fig. 2. Furthermore, on panel (iii) in Fig. 5 all the resonances reconstructed by means of the $\text{FPT}^{(-)}$ are observed to lie outside the unit circle ($|z| > 1$), as expected. A careful inspection reveals that the k th heights $|d_k^\pm|/\text{Im}(\nu_k^\pm)$ shown on panels (ii) in Figs. 4 and 5 do not fully match the corresponding tops of the k th peaks in the component shape spectra $d_k^\pm z^{\pm 1}/(z - z_k^\pm)$ from panel (v). This is explained by the fact that the heights $|d_k^\pm|/\text{Im}(\nu_k^\pm)$ are due to the line-shapes $d_k^\pm/(\omega - \omega_k^\pm)$ rather than to the presently adopted spectra $d_k^\pm z^{\pm 1}/(z - z_k^\pm)$. The former and the latter line-shapes are given in terms of the angular frequencies $\{\omega, \omega_k^\pm\}$ and harmonic variables $\{z^{\pm 1}, z_k^{\pm 1}\}$, respectively, where $z^{\pm 1} = \exp(\pm i\omega\tau)$ and $z_k^{\pm 1} = \exp(\pm i\omega_k\tau)$.

In Fig. 6 we display the absorption component shape spectra (left column) and total shape spectra (right column) from the $\text{FPT}^{(-)}$ computed near full convergence at 3 partial signal lengths $N_P = 180, 220, 260$. The three panels on the right column for the total shape spectra have all reached full convergence. However, on the left column for the corresponding component shape spectra, full convergence is achieved only at $N_P = 220, 260$. On panel (i) for the component shape spectra at $N_P = 180$, peak $n_k^\circ = 11$ is absent, and peak $n_k^\circ = 12$ is over-estimated. Furthermore, the area of the 12th peak is over-estimated by the amount of the area of the absent 11th peak. As a consequence of this latter compensation, the total shape spectrum has not reflected that either shortcoming had occurred. Namely, the total shape spectrum on panel (iv) for $N_P = 180$ reached complete convergence even though peak $n_k^\circ = 11$ was missing and peak $n_k^\circ = 12$ was over-estimated. We verified that this full convergence is also conformed by the corresponding zero-valued spectra for the residual $\text{Re}(P_{\bar{K}}/Q_{\bar{K}})[N] - \text{Re}(P_{\bar{K}}/Q_{\bar{K}})[N_P]$ ($N = 1024, N_P = 180, 220, 260$). We have also verified that the corresponding three consecutive difference spectra on panels: $\text{Re}(P_{\bar{K}}/Q_{\bar{K}})[220] - \text{Re}(P_{\bar{K}}/Q_{\bar{K}})[180]$, $\text{Re}(P_{\bar{K}}/Q_{\bar{K}})[260] - \text{Re}(P_{\bar{K}}/Q_{\bar{K}})[220]$ and $\text{Re}(P_{\bar{K}}/Q_{\bar{K}})[260] - \text{Re}(P_{\bar{K}}/Q_{\bar{K}})[180]$ (not shown). These differences were all found to be identical to each other, despite the lack of convergence of the component shape spectrum from panel (i). Hence, we can conclude that while obtaining the residual or error spectra at the level of background noise may be a necessary condition, this is not sufficient for judging the reliability of estimation in practice. Therefore, it is recommended to pass beyond the point where full convergence of the total shape spectra has been reached for the first time (in this case above $N_P = 180$) in order to verify that anomalies as seen on panels (i) and (iv) of Fig. 6 do not occur in the final results. Such final results obtained for $N_P = 220$ and 260 are displayed on panels (ii) and (iii) in Fig. 6 for the components as well as panels (v) and (vi) for the envelopes. Clearly, for consistency, monitoring the stability of the component spectra should be done together with the inspection of the constancy of the reconstructed genuine spectral parameters.

Robustness and stability of reconstructions in the fast Padé transform stems from the capability of this method to unambiguously disentangle genuine from spurious information in signal processing. A clear illustration of this separation is given in Fig. 7 by identifying spurious or Froissart doublets through their coincident poles and zeros. Although genuine poles and zeros are not confluent, they nevertheless could be very close to each other, as is indeed seen in some of the physical resonances shown in Fig. 7. The question then arises as to how to unequivocally separate genuine from spurious resonances in such difficult cases. The answer is in the stability of genuine versus the instability of spurious resonances. Irrespective of the smallness of a pole-zero distance for genuine resonances, they will always remain stable against e.g. changing the order/rank of the FPT, when going from one diagonal to another in the Padé table or altering the partial signal length or adding a small amount of random Gaussian white noise, etc. By contrast, any similar changes will yield marked instability of spurious poles and zeros, so that they will roam around in the complex frequency plane, near the natural locations of noise in the vicinity of the unit circle, $|z| = 1$, as in Fig. 7.

EXACT QUANTIFICATION by FAST PADE TRANSFORM INSIDE the UNIT CIRCLE, FPT⁽⁺⁾; FID LENGTH : $N_p = 256$

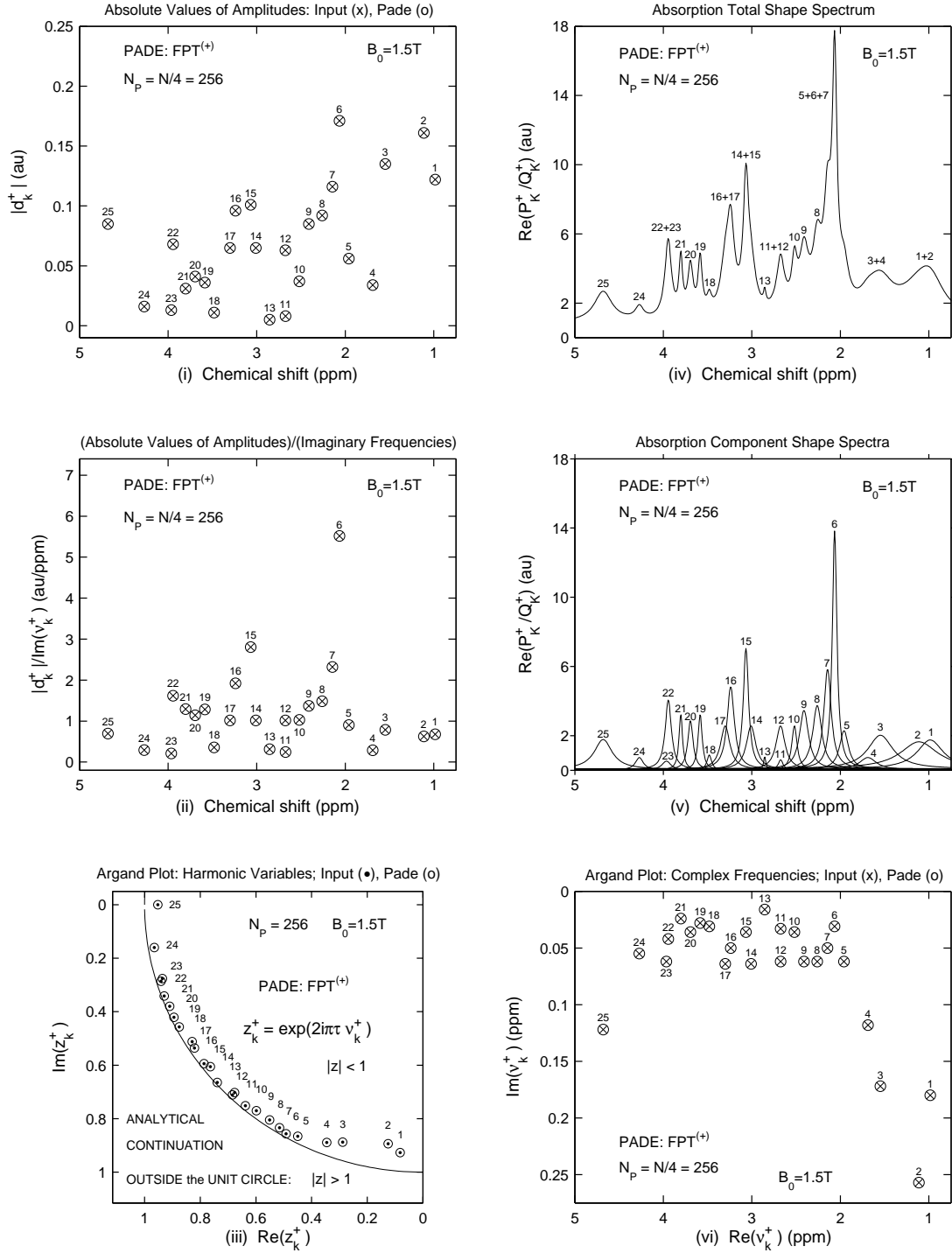


Figure 4: Configurations of the reconstructed spectral parameters in the FPT⁽⁺⁾. Panel (i): the absolute values $|d_k^+|$ of the amplitudes d_k^+ at the corresponding chemical shifts, $\text{Re}(v_k^+)$. Panel (ii): the ratios $|d_k^+|/\text{Im}(v_k^+)$ that are proportional to the peak heights. Panel (iii): distributions of poles via the harmonic variable z_k^+ in the complex z^+ -plane. Panel (vi): distributions of the fundamental complex frequencies v_k^+ in the complex v^+ -plane.

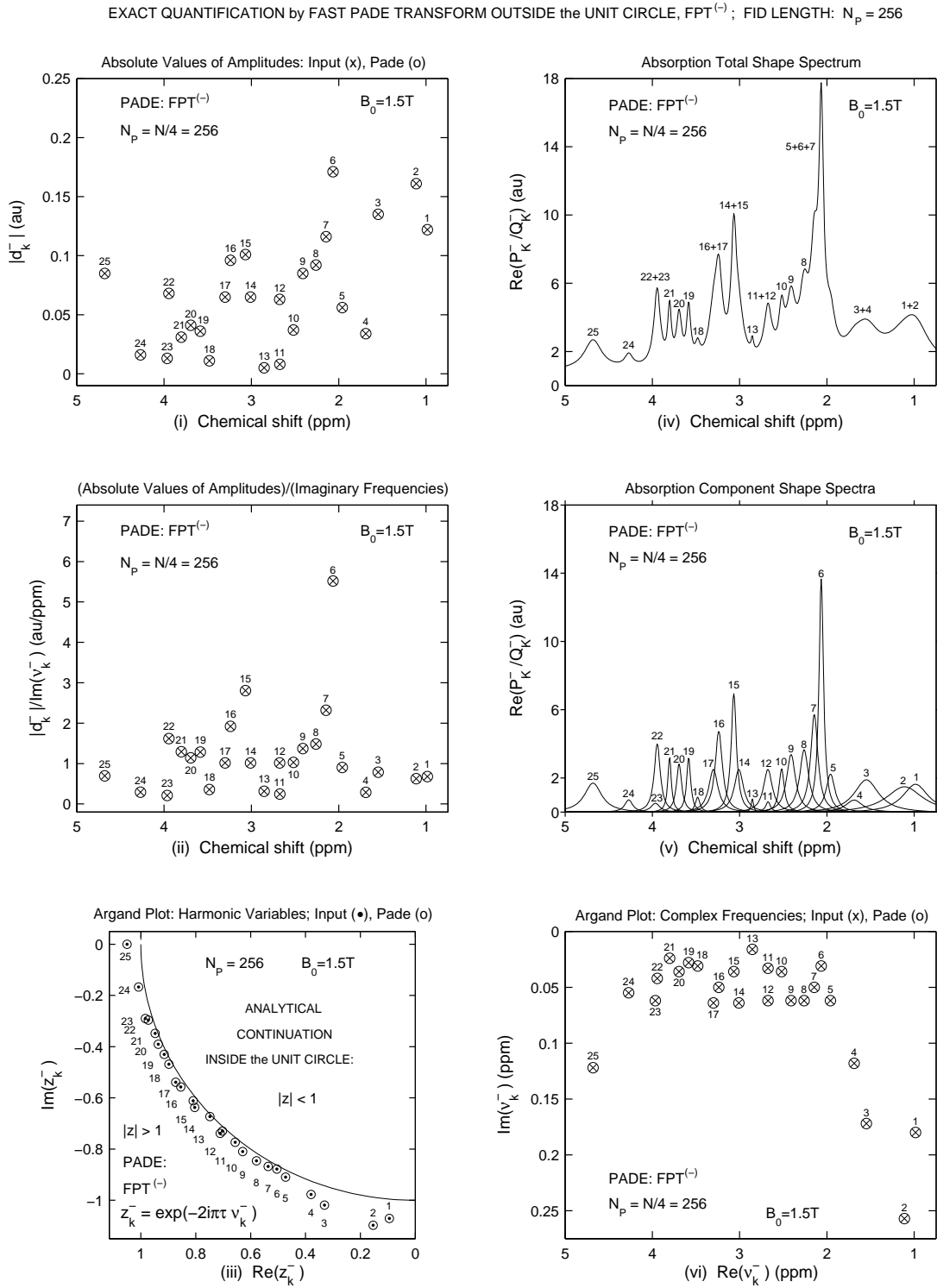


Figure 5: Configurations of the reconstructed spectral parameters in the $FPT^{(-)}$. Panel (i): the absolute values $|d_k^-|$ of the amplitudes d_k^- at the corresponding chemical shifts, $Re(\nu_k^-)$. Panel (ii): the ratios $|d_k^-|/Im(\nu_k^-)$ that are proportional to the peak heights. Panel (iii): distributions of poles via the harmonic variable z_k^- in the complex z^- -plane. Panel (vi): distributions of the fundamental complex frequencies ν_k^- in the complex ν^- -plane.

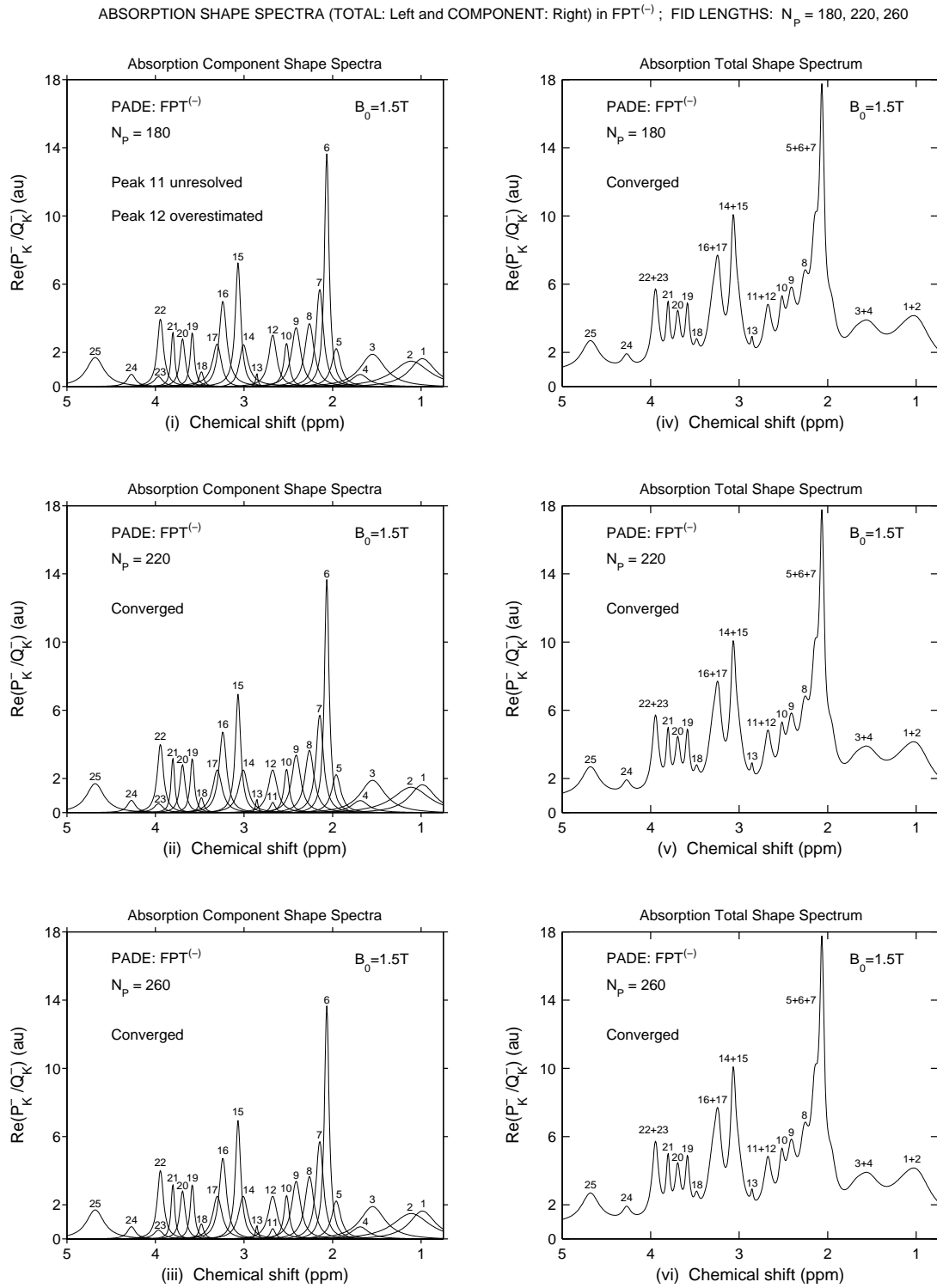


Figure 6: Absorption component shape spectra (left) and absorption total shape spectra (right) from the $FPT^{(-)}$ near full convergence for signal lengths $N_p = 180, 220, 260$. On panel (iv) for $N_p = 180$, the total shape spectrum reached full convergence, despite the fact that, on panel (i) for the corresponding component shape spectra, the 11th peak is missing and the 12th peak is over-estimated.

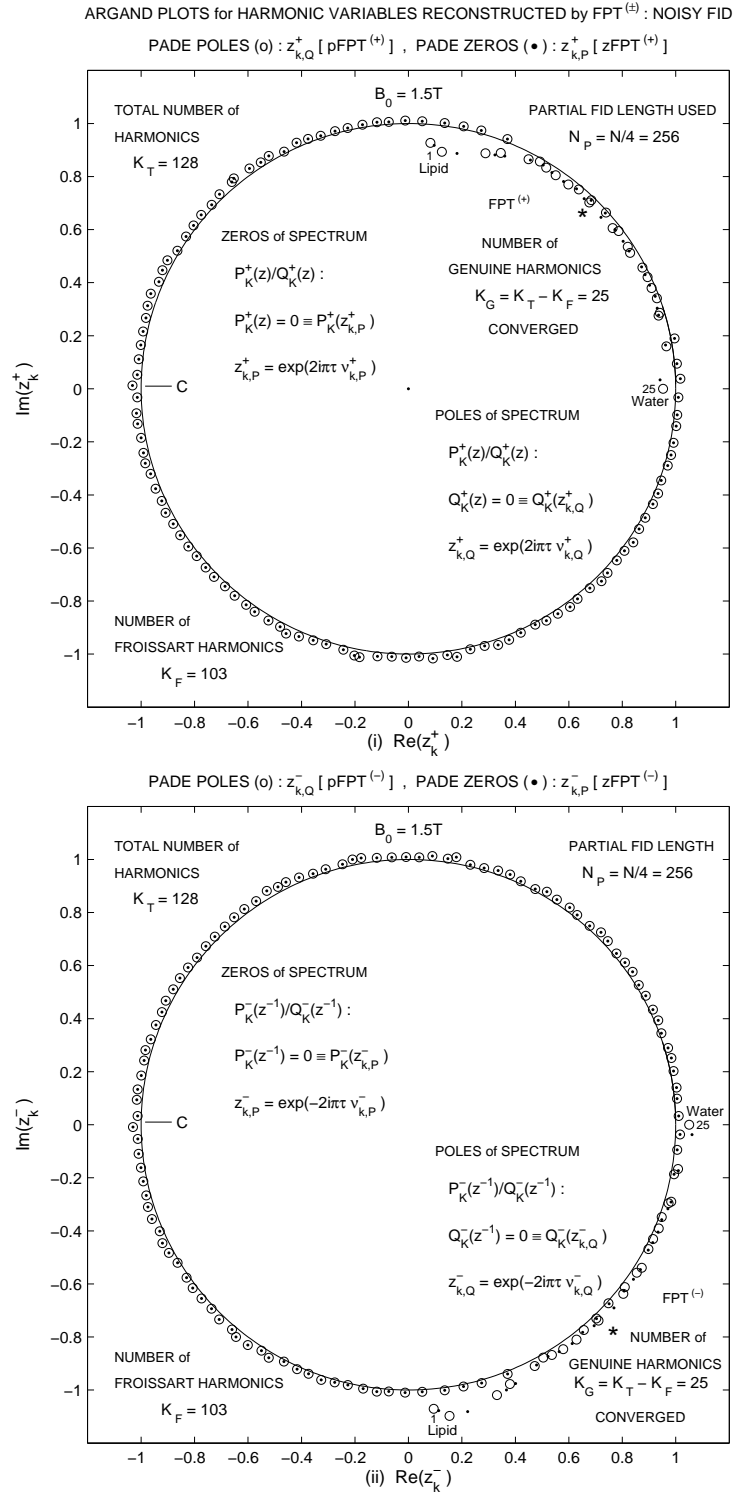


Figure 7: Froissart doublets for unequivocal signal noise-separation which yields exact reconstruction of the true number K_G of genuine resonances by the FPT⁽⁺⁾ (top) and FPT⁽⁻⁾ (bottom). Complex-valued, random zero-mean Gaussian noise of standard deviation 0.00275RMS is added to the noiseless FID (RMS is the root mean-square of the noise-free FID). All spurious resonances are located outside the unit circle. As such, a complete separation of spurious and genuine resonances is achieved by the FPT⁽⁺⁾. Although spurious and genuine resonances are mixed together in the FPT⁽⁻⁾, only the former have confluent poles and zeros. The star symbol on both panels points to the two closest resonances ($n_k^o = 11$ and $n_k^o = 12$) whose chemical shifts differ by 0.001 ppm.

As such, Froissart or spurious resonances are not recognized merely through pole-zero coincidences and the ensuing zero or near-zero amplitudes, but also via their noticeable instability relative to the persistent stability of genuine resonances. For noisy time signals, spurious poles and zeros cannot coincide exactly, as opposed to the noiseless FID. Therefore, one can certainly have a situation, where a distance between a pole and a zero is so small that it would be tempting to identify the underlying resonance as spurious. However, this might be incorrect. What is additionally needed for a convincing separation of spurious from genuine information is to test stability of the retrieved pole-zero couples by varying the degree of the Padé polynomials or by gradually increasing the partial signal length, etc. If the reconstructed pole-zero pair emerges as stable, it would be associated with a genuine resonance. Otherwise, it would represent a spurious resonance, i.e. a Froissart doublet. In this way, uniquely within the $\text{FPT}^{(+)}$ and $\text{FPT}^{(-)}$, Froissart doublets can be used to determine the exact number K_G of genuine resonances, as illustrated in Fig. 7, both inside $|z| < 1$ and outside $|z| > 1$ the unit circle.

4 Conclusion

The Padé approximant (PA), as a ratio of two polynomials, is the most known rational function. In physics, this polynomial quotient represents the finite rank representation of the Green function or the energy spectrum of a general system. Energy or frequency spectra of a generic system are completely described by the fundamental sets of all the physical poles and zeros. Such key characteristics are directly ingrained in the very form of the PA, because its numerator and denominator polynomial give rise to the system zeros and poles, respectively. In spectral analysis and signal processing, the PA is equivalently called the fast Padé transform (FPT). This was done to make an implicit reference to the integral transformation from the originally measured time domain to the subsequently analyzed frequency domain information. The most often employed qualitative method for this type of transformation has been the fast Fourier transform (FFT), which is commercially built into spectrometers for physics and chemistry as well as in magnetic resonance scanners for medicine.

The FFT provides only an overall total shape spectrum in the frequency domain, which represents an envelope of all concentrations of molecules in the structural studies of matter. The goal, however, is precisely to extract the information which is underneath this envelope, namely the component spectrum for each molecule. Since this is impossible within the Fourier analysis, the customary procedure has been to resort to fitting the total shape spectrum from the FFT by adjusting the entire envelope to a subjectively pre-selected number of components. The number of molecules and their abundance or concentrations are estimated in post-processing the given FFT spectrum via least square fitting. The major drawback of this usual procedure in signal processing is the lack of uniqueness, since any number of pre-assigned peaks can be fitted to a given envelope within a prescribed accuracy. This procedure has not met with success in the interdisciplinary applications because some physical molecules can be missed and unphysical ones falsely predicted. Moreover, due to its linearity, the FFT imparts noise as unaltered from the time domain to the frequency domain. The FFT has no possibility of separating noise from the true signal. Each molecule has one or more resonant frequencies. Besides concentrations, the task is also to reconstruct these frequencies, known as chemical shifts. The FFT cannot retrieve them, since this method deals with the preassigned Fourier grid frequencies as a function of the total acquisition time. This is the main reason for which post-processing the envelopes from the FFT is used by means of fitting to surmise the underlying components.

On the other hand, the fast Padé transform, the FPT, simultaneously circumvents all these drawbacks of the FFT. As a non-linear transform, the FPT effectively suppresses noise from the analyzed time signals. Most importantly, the FPT avoids post-processing altogether via fitting or any other subjective adjustments. This is accomplished by a direct quantification of the time signal through exact spectral analysis, which provides the unique solutions with machine accuracy for the inverse harmonic problem. This solution contains four spectral parameters (two complex frequencies and two complex amplitudes) for each resonance or peak in the associated frequency spectrum. From such spectral parameters, the molecular concentrations are unequivocally extracted, thus bypassing the ubiquitous ambiguities from fittings (under-fitting associated with missing genuine molecules and over-fitting corresponding to finding unphysical resonances). Moreover, the FPT succeeds in solving the most difficult problem in spectral analysis of time signals corrupted with noise by providing the exact separation of signal from noise. Identification of noise and noise-like information is achieved in the FPT through the appearance of Froissart doublets where poles and zeros coincide in the analyzed spectrum. As a double signature for signal-noise separation, the FPT detects zero amplitudes for Froissart doublets. In this way, genuine and spurious resonances are unambiguously disentangled within the FPT.

The expounded features of the fast Padé transform have been confirmed in practice for both theoretically generated and experimentally measured time signals. In the present work, we provide the proof-of-principle as a supporting evidence for machine accurate reconstructions that are robust even against the computational round-off-errors. For concreteness, the concept of the versatile and powerful Padé methodology and illustrations are presented specifically

for time signals encountered the field of nuclear magnetic resonance spectroscopy. However, there is no limitation for wide applications of the fast Padé transform to any other field dealing with time signals and spectra. Whenever the fast Fourier transform and the accompanying fitting are employed with all their ensuing ambiguities as obvious drawbacks, the fast Padé transform can come as the rescue to carry out spectral analysis for reconstruction of the hidden information from the studied substance through reliable extraction of spectral parameters of all the genuine resonances, including their true number.

Acknowledgment

This work was supported by the Swedish Cancer Society Research Fund (Cancerfonden), King Gustav the Fifth's Jubilee Foundation and the Karolinska Institutet Research Fund.

References

- [1] Günther H 2001 *NMR Spectroscopy*, 2nd Edn (John Willey & Sons: Chichester)
- [2] Belkić Dž 2005 *Quantum-Mechanical Signal Processing and Spectral Analysis* (Institute of Physics Publishing: Bristol)
- [3] Belkić K 2004 *Molecular Imaging through Magnetic Resonance for Clinical Oncology* (Cambridge International Science Publishing: Cambridge)
- [4] Belkić Dž and Belkić K 2010 *Signal Processing in Magnetic Resonance Spectroscopy with Biomedical Applications* (Taylor & Francis: London)
- [5] de Graff R A 2010 *In Vivo NMR Spectroscopy: Principles and Techniques* (John Willey & Sons: Sussex)
- [6] Mountford C E, Doran S, Lean C L and Russell P 2004 *Chem. Rev.* **104** 3667
- [7] Delsuc M A, Ni F and Levy G C 1987 *J. Magn. Reson.* **73** 548
- [8] Zhu G and Bax A 1992 *J. Magn. Reson.* **100** 202
- [9] Alejos Ó, de Francisco C, Hernández P and Muñoz 1997 *Comput. Mater. Sci.* **7** 169
- [10] Chen R, Ma G and Guo H 2000 *Chem. Phys. Lett.* **320** 567
- [11] Levitina T V and Brändas E J 2001 *Comput. Chem.* **825** 55
- [12] Taswell T 2000 *J. Comput. Appl. Math.* **121** 179
- [13] Jentschura U D 2000 *Phys. Rev. D* **62** 076001
- [14] Caliceti E, Meyer-Hermann M, Ribeca P, Surzhykov A and Jentschura U D 2007 *Phys. Rep.* **446** (2007) 1
- [15] Belkić Dž 2004 *Nucl. Instr. Meth. Phys. Res. A* **525** 366
- [16] Belkić Dž and Belkić K 2006 *Phys. Med. Biol.* **51** 1049
- [17] Belkić Dž and Belkić K 2009 *J. Math. Chem.* **45** 819
- [18] Feifel R, Ueada K, de Fanis A, Okada K, Tanimoto S, Furuta T, Shindo H, Kitajima M, Tanaka H, Björnholm O, Karlsson L, Svensson S and Sorensen S L 2003 *Phys. Rev. A* **67** 032504
- [19] Takahashi O, Matsuyama K, Tabayashi K and Yamasaki K 2009 *J. Phys. B: At. Mol. Opt. Phys.* **42** 245102
- [20] Froissart M 1989 *CNRS, Recherche Cooperative sur Programme N° 25, Strasbourg*, Carmona J, Froissart M, Robinson D W and Ruelle D (Eds) **9** 1
- [21] Gilevicz J and Kryakin Y 2003 *J. Comput. Appl. Math.* **153** 235
- [22] Frahm J, Bruhn H, Gyngell M L, Merboldt K D, Hänicke W and Sauter R 1989 *Magn. Reson. Med.* **9** 79